Tissue Engineering

DOI: 10.1089/ten.TEA.2018.0271

CRISPR/Cas9 edited hiPSC-based vascular tissues to model aging and disease-dependent impairment

Aylin Acun[1], Pinar Zorlutuna*[1, 2]

1. Bioengineering Graduate Program, University of Notre Dame, IN

2. Aerospace and Mechanical Engineering Department, University of Notre Dame, IN

Aylin Acun

225 Multidisciplinary Research Building, Notre Dame, IN, 46556

Email: aacun@alumni.nd.edu

Phone: 860 690 8087

Pinar Zorlutuna (corresponding author)

143 Multidisciplinary Research Building Notre Dame, IN, 46556

Email: Zorlutuna.1@nd.edu

Phone: 574-631-8543

* Corresponding author

Tissue Engineering
CRISPR/Cas9 edited hiPSC-based vascular tissues to model aging and disease-dependent impairment (DOI: 10.1089/ten.TEA.2018.0271)
This paper has been peer-reviewed and accepted for publication, but has yet to undergo copyediting and proof correction. The final published version may differ from this proof.

Abstract

The discovery of induced pluripotent stem cells (iPSCs) and advancements in genome editing technology introduced a new perspective to disease modeling as genetic factors can now be incorporated to mimic the pathology of interest. Ischemia and age-driven impairment of endothelium is one of the very important factors in the prognosis of many diseases as it leads to decreased angiogenic response and is shown to be related to age-dependent decrease in HIF-1α expression levels in endothelial cells. However, there are no models that show the characteristic age and ischemia-driven deterioration of the endothelium with both the functional and genetic mimicry. Here, we developed a 3D in vitro tissue model comprised of human-origin iPSC-derived endothelial cells (iECs) which were CRISPR/Cas9 edited for *HIF-1A* knockout. Confirmed with a significant decrease in HIF-1α mRNA and protein content, our CRISPR/Cas9 edited tissue models showed disrupted oxygen-controlled stabilization of HIF-1α evidenced by decreased viability, 2D tube formation and 3D lumen formation along with increased mitochondrial ROS accumulation under ischemia, mimicking the age-driven impairment in endothelial function. hiPSC-based tissue and disease models such as the one presented here are promising to study human disease in a physiologically and pathologically-relevant manner and to develop new therapies.

Impact Statement

Modeling human disease as precisely as possible is of upmost importance in understanding the underlying pathology and discovering effective therapies. Therefore, disease models that are highly controlled and comprised of human-origin cells that present the disease phenotype are crucial. The hiPSC-based tissue model we present here is an important example of human-origin tissue model with controlled gene expression. Through CRISPR/Cas9 editing of HIF-1α in hiPSCs, we developed tissue models that show the age and disease-dependent endothelial deterioration. This model holds promise for various biomedical applications as more realistic disease phenotypes can be created using fully human-origin platforms.

Tissue Engineering
CRISPR/Cas9 edited hiPSC-based vascular tissues to model aging and disease-dependent impairment (DOI: 10.1089/ten.TEA.2018.0271)
This paper has been peer-reviewed and accepted for publication, but has yet to undergo copyediting and proof correction. The final published version may differ from this proof.

Introduction

Development of effective treatments for human diseases is only possible through a detailed understanding of the genetic and environmental factors contributing to each disease condition precisely. Although animal models are inevitably essential for safety testing and understanding the systemic response, the evident differences between different species render it difficult to solely depend on this data for developing effective treatments. Hence, engineered tissue models using human cells have been investigated as an alternate and complementary platform. However, not all human cell types are readily available and the human adult stem cells have limited differentiation potential. Luckily, reprogrammed cells, called induced pluripotent stem cells (iPSCs), carry the potential to form all 3 germ layers and can subsequently be directed to various lineages via manipulation of different molecular pathways.

Following their discovery, the iPSCs rapidly found many applications in tissue and disease modeling and the use of various genome editing technologies broadened their applications. Through genome editing, precise mutations can be introduced or can be corrected for understanding the function of a gene as well as investigating potential therapies for genetic diseases. Clustered regulatory interspaced short palindromic repeat (CRISPR)/Cas9 endonuclease technology is one of the most preferred methods of gene editing of the iPSCs. The site recognition for DNA binding of this nuclease is guided by RNA sequences, avoiding the need for the nuclease itself to be redesigned for each target. Therefore, the ease of designing different RNA sequences as well as the ability to target multiple sequences simultaneously has led to the wide use of CRISPRs[1,2]. CRISPR/Cas9-mediated genome editing has been used in correcting or modeling various diseases in vivo[3] and in vitro such as cataract[4], tyrosinemia[5], polycystic kidney disease[6], chronic granulomatous disease[7], Barth syndrome[8] and Huntington's disease[9].

Ischemia is an important risk factor in development and prognosis of many diseases. Hypoxia inducible factor 1 (HIF-1), a heterodimeric transcription factor, is known to be a major player in oxygen homeostasis in cells and tissues[10–12]. It is composed of HIF-1α and

Tissue Engineering
CRISPR/Cas9 edited hiPSC-based vascular tissues to model aging and disease-dependent impairment (DOI: 10.1089/ten.TEA.2018.0271)
This paper has been peer-reviewed and accepted for publication, but has yet to undergo copyediting and proof correction. The final published version may differ from this proof.

HIF-1β subunits, which dimerize in the nucleus following the nuclear localization of HIF-1α subunit, under hypoxia. This oxygen-dependent regulation renders HIF-1α crucial for tissues' adaptation to ischemia and for induction of angiogenesis[13]. Involvement of HIF-1 has been shown in various disease pathologies, including but not limited to myocardial ischemia[14–17], cerebral ischemia[18–20], renal ischemia[21,22], and hind limb ischemia[23]. Importantly, impaired angiogenic response observed with age as well as damage or ischemia-induced endothelial dysfunction has been linked to HIF-1 activity. Ahluwalia and colleagues reported that the declined nuclear localization of HIF-1α in microvascular endothelial cells leads to age-related impairment of angiogenesis[24]. In another study, Chang et al. used a murine skin flap model and showed that in aged animals, neovascularization was impaired due to significant decline in endothelial progenitor cell recruitment to the ischemic area. They showed that the age-dependent decrease in HIF-1α stabilization was involved in lower endothelial cell recruitment[25]. Therefore, HIF-1α expression, especially in endothelial cells (ECs), is an important factor to consider when modeling ischemic diseases, most of which primarily affect the elderly population.

In this study, we developed human iPSC-based 3D tissue models showing the age and disease-dependent impaired endothelial function, represented with decreased viability, angiogenesis, and stress response through knocking out HIF-1α. To do so, we used CRISPR/Cas9 editing to create HIF-1α knockout hiPSC lines. We have successfully introduced homozygous and heterozygous deletions in *HIF-1A* and observed that these cell lines maintained their pluripotency and differentiation potential. Two cell lines with 19 (HIF-1$\alpha^{\Delta 19}$) and 42 (HIF-1$\alpha^{\Delta 42}$) base pair (bp) homozygous deletions in the second exon of *HIF-1A* were then differentiated to ECs. Both 2D culture and the 3D model tissues of the CRISPR/Cas9 edited iECs showed lower angiogenic potential and viability as well as an increased mitochondrial ROS accumulation, showing similarities to functional deterioration observed in age-related and ischemia-induced vascular diseases. Overall, our results present that combining iPSC technology with CRISPR/Cas9 editing, it is possible to develop tissue models with impaired angiogenic response through disrupting the oxygen-dependent stabilization of HIF-1α. Such tissue models are important for studying the aged

vascular microenvironment and progress of ischemic diseases within, as well as for developing novel therapies for their treatment.

Tissue Engineering
CRISPR/Cas9 edited hiPSC-based vascular tissues to model aging and disease-dependent impairment (DOI: 10.1089/ten.TEA.2018.0271)
This paper has been peer-reviewed and accepted for publication, but has yet to undergo copyediting and proof correction. The final published version may differ from this proof.

Materials and Methods

Cell Culture: Human Umbilical Vein Endothelial Cells (HUVECs) (Lonza, CC-2935) were maintained in endothelial growth medium (EGM, Lonza, Endothelial Growth Medium Plus) with media changes every 2 days. HUVECs were used at passages 4 to 8 and passaged using 0.05% trypsin-EDTA as needed. For all experiments HUVECs were used as positive controls. DiPSC-1016SevA line of human induced pluripotent stem cells (hiPSCs), derived from skin fibroblasts, were kindly provided by Dr. K. Musunuru and Dr. C. Cowan, Harvard University. The cells were cultured on Geltrex (Life Technologies) coated tissue culture dishes in mTeSR-1 culture medium (Stemcell Technologies) with daily media changes. The cells were passaged every 3-4 days using Accutase (Stemcell Technologies). The undifferentiated phenotype of the hiPSCs was observed daily using a light microscope (Leica).

CRISPR/Cas9 editing of iPSCs for HIF-1α knockout: The genetically edited cell lines were created using CRISPR/Cas9 genome-editing system which is comprised of the Cas9 nuclease and a guide RNA (17-20 nucleotide long) that has a 5' NGG (PAM sequence). We designed CRISPR guide RNAs that target *HIF-1A* gene, in silico. The plasmids encoding the guide RNAs and Cas9 were then prepared using the established protocols[26]. The plasmids were then introduced to hiPSCs using electroporation. The cells with successful delivery of the plasmids were then enriched using FACS making use of the GFP sequence in Cas9 plasmid. The enriched cells were then seeded as single cells and allowed to grow to form colonies. At least 192 colonies were picked from each electroporation and expanded with duplicates frozen for further expansion of the knockout clones. Next, genomic DNA was collected from all colonies and used for PCR amplification of the target DNA. The changes in the target DNA was assessed by gel electrophoresis. Then, by direct sequencing of the PCR products with altered genome the specific site and length of the deletion was determined using APE software.

Endothelial differentiation of HIF-1α knocout iPSCs: We have selected 2 cell lines, with 19 bp (HIF-1$\alpha^{\Delta 19}$) and 42 bp (HIF-1$\alpha^{\Delta 42}$) deletions in the second exon of HIF-1α. These cell lines

Tissue Engineering
CRISPR/Cas9 edited hiPSC-based vascular tissues to model aging and disease-dependent impairment (DOI: 10.1089/ten.TEA.2018.0271)
This paper has been peer-reviewed and accepted for publication, but has yet to undergo copyediting and proof correction. The final published version may differ from this proof.

are collectively referred to as HIF-1α knockout cell lines (HIF-1α$^{\Delta}$) throughout the manuscript. In order to differentiate the HIF-1α wild type (HIF-1α^{WT}) and knockout hiPSC lines to endothelial lineage we used a previously established protocol[27]. Briefly, the hiPSCs were induced to differentiation by culturing in media supplemented with a glycogen synthase kinase 3β (GSK3β) inhibitor, CHIR, and bone morphogenic protein 4 (BMP4) (R&D Systems). The media was replaced with StemPro-34 SFM medium (Life Technologies) (supplemented with 200ng/mL VEGF and 2 μM forskolin) after three days. At the end of day six, the iPSC-derived endothelial cells (iECs) were sorted using fluorescence activated cell sorting (BD Biosciences, FACSAria III - Fluorescence Assisted Cell Sorter, IU School of Medicine, South Bend Imaging and Flow Cytometry Core facility) against vascular endothelial cadherin (VE-CAD). The sorted cells were seeded on fibronectin coated plates and maintained in EGM with media changes every 2 days. Cells were accepted to be passage 0 right after sorting. For all experiments iECs of passage 6 to 9 were used and they were collected for experiments using 0.05% trypsin-EDTA (Life technologies) at approximately 80% confluency.

Quantitative Real-Time Polymerase Chain Reaction (qRT-PCR): To determine the HIF-1α mRNA amount RNA was collected from iPSCs and iECs maintained at normoxia (21% O_2, 5% CO_2 at 37°C) or hypoxia (1% O_2, 5% CO_2 at 37°C) for 24 h using a total RNA isolation kit (RNeasy, Qiagen). To determine the mRNA expression levels of endothelial markers CD31, endothelin 1 (EDN1), and von Willebrand factor (vWF), total RNA was collected from iECs maintained under normoxia. NanoDrop 2000 Spectrophotometer (Thermo Fisher Scientific) was used to determine the RNA purity and concentration. The respective cDNA was prepared using the iScript cDNA Synthesis Kit (Bio-Rad). qRT-PCR reactions were run on CFX Connect 96 Real-Time PCR system (Bio-Rad) using iTaq SYBR Green Supermix (Bio-Rad). The primers used in these experiments are listed in Supplementary Table 1. The mRNA expression of target proteins was normalized to GAPDH expression and the relative expression of genes was quantified by the ΔΔCt method through Bio-Rad CFX Manager software. All PCR reactions were run in triplicates. (n=3)

Enzyme-linked immunosorbent assay (ELISA): Total protein was collected from iPSCs and iECs maintained at normoxia (21% O_2, 5% CO_2 at 37°C) or hypoxia (1% O_2, 5% CO_2 at 37°C)

for 24 h using cell lysis buffer (CelLytic M, Sigma-Aldrich) supplemented with a protease inhibitor cocktail (10% v/v) (Sigma-Aldrich). HIF-1α protein quantification was done using HIF-1-alpha Human SimpleStep ELISA™ Kit (Abcam) using the protein extracts, following manufacturer's instructions. Total protein amount for each sample group was determined using BCA assay (Pierce™ Rapid Gold BCA Protein Assay Kit, Thermo Fisher) for normalization. The respective blank measurements were subtracted from all BCA and ELISA measurements and the total protein and HIF-1α concentrations were calculated referring to the respective calibration curves (data not shown). (n=3)

Immunostaining: iECs were fixed with 4% paraformaldehyde (10 min at RT) followed by washing with PBS 3 times. The cells were then blocked using 10 % goat serum (1h at RT) and then incubated with rabbit anti-human VE-CAD antibody (Abcam, ab33168) at a 1:100 dilution, for 4 h at 4°C. The primary antibody was washed with PBS 3 times and the samples were incubated with the species-specific secondary antibody (goat anti-rabbit Alexa Fluor 594, Thermo Fisher) at a 1:200 dilution for 4 h at 4°C. The samples were washed until there was no background signal and the nuclei were stained with DAPI (5 min, RT) (Life Technologies). The respective images were acquired using a fluorescence microscope (Zeiss, Hamamatsu ORCA flash 4.0). (n=3)

Tube formation assay: Chilled 48 well plates were coated with a thick layer of Geltrex (Life Technologies) (100 µL/cm^2) and incubated at 37°C for 30 min to achieve gelation. Then HUVECs and iECs were seeded on the Geltrex coated wells at a density of 40x10^3 cells/well and incubated overnight under normoxia (21% O_2, 5% CO_2 at 37°C) or hypoxia (1% O_2, 5% CO_2 at 37°C) for tube formation. The samples were then stained with Calcein-AM (Thermo Fisher) for 15 mins at 37°C and imaged at lowest magnification using a fluorescence microscope (Zeiss, Hamamatsu ORCA flash 4.0). Through using the lowest magnification, the whole wells were captured with 5 images and the number of tubes was determined by counting the fully-closed sections of endothelial cells in each image using imageJ software and represented as the average number of tubes per well. (n≥6)

Scratch assay: The HUVECs and iECs were seeded on 24 well plates at 100% confluency. Scratches were made using a 200 µL pipette tip and the cells were washed with PBS to

Tissue Engineering
CRISPR/Cas9 edited hiPSC-based vascular tissues to model aging and disease-dependent impairment (DOI: 10.1089/ten.TEA.2018.0271)
This paper has been peer-reviewed and accepted for publication, but has yet to undergo copyediting and proof correction. The final published version may differ from this proof.

remove cell debris. Then the media was replaced with EGM without serum to avoid cell proliferation. The scratch area was imaged right after introducing the scratches (T=0h) and after 18 h of incubation (T=18h) at 5 different locations along the scratches. The cells were stained with Calcein-AM for 15 min at 37°C before each time point. The initial scratch positions were labeled by putting marks outside of the well plates and at the end of 18 h the original scratch points were determined referring to the marks. The experiment was conducted under normoxia and hypoxia. Hypoxic conditions were created through incubation at 1% O_2 using an oxygen-controlled incubator. The EGM used with these samples was equilibrated to 1% O_2 through overnight incubation in the oxygen-controlled incubator, the night before the scratches were introduced. (n=6)

Ischemia treatment in 2D culture: In order to examine the ischemia response of HIF-1α^{WT}, HIF-1$\alpha^{\Delta 19}$, and HIF-1$\alpha^{\Delta 42}$ iECs on 2D the cells were seeded to 96 well plates in triplicates at a seeding density of $20x10^3$ cells/well. After overnight incubation to allow cell attachment, ischemia treatment was started by exchanging the media to hypoxia equilibrated media. The ischemia samples were then immediately placed in the hypoxic incubator and maintained there for 96 hours. Media was changed after 48 hours using hypoxia equilibrated media. The media exchange was done under normoxic conditions to preserve aseptic conditions and was completed within under one minute, this without exposing the cells to normoxia for prolonged time periods. (n=6)

Fabrication of 3D model tissues and ischemia treatment: 3D model tissues were fabricated by encapsulating the iECs in methacrylated gelatin (GelMA) (10% w/v) supplemented with 0.05% photoinitiator (Irgacure2959, Sigma Aldrich). GelMA was synthesized following a previously established protocol[28]. iECs were mixed with GelMA at a 1:1 ratio and then sandwiched between a plastic surface and a glass slide and exposed to 6.9 mW/cm^2 UV irradiation for 30 s. The crosslinked constructs were washed with PBS once for 1 minute and then 3 times with culture media for 15 min each time. The ischemia treatment was then started by exchanging the media with hypoxia equilibrated media. The media was hypoxia equilibrated by incubating the media in hypoxic incubator (1%O_2) overnight. The media change was performed under normoxia then the tissues were maintained under hypoxia (1% O_2, 5% CO_2 at 37°C) for 96 hours with media change at 48

hours, as explained in the previous section. The normoxia controls were maintained under normoxic conditions (21% O_2, 5% CO_2 at 37°C) for 96 hours and received media changes at the same time points. (n=3)

Live/Dead assay and Mitochondrial ROS assay: The 2D cultures and 3D tissues were stained with Live/Dead assay (Life Technologies) at the end of 96 hours normoxia or hypoxia culture, following the manufacturer's instructions. The 2D cultures were imaged using a fluorescence microscope (Zeiss, Hamamatsu ORCA flash 4.0) at 5 different locations of each well. The 3D tissues were imaged using a fluorescence microscope (Zeiss, Hamamatsu ORCA flash 4.0) by taking z-stack images in at least 3 positions of each tissue. The z-stack images were projected to form the maximum projection at each field of view. A built-in optical sectioning tool (Apotome, Zeiss) was used during 3D imaging to remove background accumulation from different z-stack images when projected. The images of 2D cultures and the maximum projection images of 3D tissue constructs were analyzed using imageJ software to determine the number of live and dead cells. Using these numbers, the live cell percentages were quantified for each well or tissue construct. (n=3)

Lumen number and diameter quantification: The 3D constructs were maintained under normoxia or hypoxia for 14 days with regular media changes every 3 days. The constructs were imaged using a light microscope (Leica) on days 1, 3, 5, and 9 to monitor the spreading and lumen formation. On day 14 the tissues were fixed and immunostained for CD31 following the immunostaining protocol (see "immunostaining"), using mouse anti-human CD31 antibody (BD Pharmigen) at a 1:100 dilution and the species-appropriate secondary antibody (goat anti-mouse Alexa Fluor 488, Life Technologies) at a 1:200 dilution. The tissues were then imaged using a fluorescence microscope (Zeiss, Hamamatsu ORCA flash 4.0) through the thickness by taking z-stack images with 2 µm z intervals. At least 3 z-stack images were taken from each construct. The z-stack images were used for 3D reconstruction of the tissues through imageJ software volume viewer plugin. The reconstructed images were analyzed to determine lumen number and diameter by taking at least 5 slices per image. The number and diameter of lumens were calculated as the total number per construct and average±std of 6 constructs were represented. (n=3)

Tissue Engineering
CRISPR/Cas9 edited hiPSC-based vascular tissues to model aging and disease-dependent impairment (DOI: 10.1089/ten.TEA.2018.0271)
This paper has been peer-reviewed and accepted for publication, but has yet to undergo copyediting and proof correction. The final published version may differ from this proof.

Statistical analysis

The results are represented as average ± standard deviation. The statistical analysis was carried out using 1-way ANOVA analysis. Student's t-test was used for comparing two individual groups. All *p* values reported were two-sided, and statistical significance was defined as $p<0.05$. Sample size (n) was equal to or larger than 3 for all individual experiments and all experiments were repeated 3 times.

Results

CRISPR/Cas9 genome editing yields successful knockout of HIF-1α in hiPSCs

We aimed to knockout HIF-1α using the CRISPR/Cas9 genome editing. We designed 4 different CRISPR guide RNAs all targeting the second exon of HIF-1α which is the basic helix–loop–helix (bHLH) domain required for heterodimerization with HIF-1β and binding to DNA[29]. We used electroporation to introduce Cas9 plasmid including a GFP reporter along with the CRISPR guide RNAs. We achieved an electroporation efficiency of approximately 4% (Figure 1A).

Through screening the GFP positive colonies which were grown and expanded from single cells (Figure 1B), we identified two homozygous hiPSC colonies with 19 and 42 bp deletions (Figure 1C). We confirmed that the deletions created were on the second exon through sequencing (Figure 1D). After expanding these colonies, we examined the effect of the deletions in mRNA expression levels in hiPSCs (Figure 1E). We observed that the HIF-1α mRNA expression level was significantly lower in the HIF-$1\alpha^{\Delta}$ hiPSC lines compared to HIF-$1\alpha^{WT}$ under hypoxia. We then determined the HIF-1α protein levels in these cell lines and observed that there was a significant decrease as a result of both 19 bp and 42 bp deletions (Figure 1F). The HIF-$1\alpha^{\Delta 19}$ cell line showed the lowest HIF-1α protein levels, being significantly lower than both the HIF-$1\alpha^{WT}$ and HIF-$1\alpha^{\Delta 42}$ (Figure 1F).

HIF-1α knockout does not interfere with endothelial cell differentiation of hiPSCs

In order to examine the effect of HIF-1α knockout in endothelial cell behavior, we differentiated the HIF-$1\alpha^{WT}$, HIF-$1\alpha^{\Delta 19}$, and HIF-$1\alpha^{\Delta 42}$ hiPSC lines to endothelial cells. The previously established protocol yielded endothelial cells from the CRISPR/Cas9 edited

Tissue Engineering
CRISPR/Cas9 edited hiPSC-based vascular tissues to model aging and disease-dependent impairment (DOI: 10.1089/ten.TEA.2018.0271)
This paper has been peer-reviewed and accepted for publication, but has yet to undergo copyediting and proof correction. The final published version may differ from this proof.

hiPSCs that resemble HUVECs biochemically and functionally (Figure 2A). The bright field images showed that both the WT and edited iECs had the characteristic morphology of endothelial cells, as can be observed through their morphological resemblance to HUVECs (Figure 2A, top). In addition, both WT and edited iECs showed significantly higher levels of CD31, EDN-1, and vWF mRNA expression (Figure 2B) compared to undifferentiated hiPSCs and showed VE-CAD protein expression (Figure 2A, middle).

Importantly, the mRNA expression levels in HIF-1$\alpha^{\Delta 19}$ of all markers tested were comparable to that of HUVECs and HIF-1α^{WT}. CD31 and vWF mRNA expression levels in HIF-1$\alpha^{\Delta 42}$ were also comparable to HUVECs and HIF-1α^{WT}, indicating that differentiation to endothelial lineage is not hindered by the CRISPR/Cas9 editing employed here. We also tested the endothelial specific functionality of WT and edited iECs. Endothelial cells form tube-like structures by stretching along and forming connections with their neighbors when seeded on a thick layer of extracellular matrix (ECM) gels. When cultured on a thick coating of Geltrex, both WT and edited iEC cell lines showed tube-like structure formation, resembling the structures formed by HUVECs (Figure 2A, bottom).

It is important to determine if the HIF-1α mRNA or protein expression levels were affected by the differentiation process. To assess that we performed qRT-PCR and ELISA to WT and edited iECs that were cultured under normoxia and ischemia. We determined that HIF-1α mRNA expression levels are significantly lower in both HIF-1$\alpha^{\Delta 19}$ and HIF-1$\alpha^{\Delta 42}$ iECs (Figure 2C). Similarly, under hypoxia, the HIF-1α protein levels were significantly lower compared to HUVECs and HIF-1α^{WT} iECs (Figure 2D). Importantly, we determined that the increase in protein levels of HIF-1α under hypoxia was not observed in HIF-1$\alpha^{\Delta 19}$ and HIF-1$\alpha^{\Delta 42}$ iECs (Figure 2E) indicating that even if HIF-1α protein is present at very low levels in these cell lines, its levels do not increase when exposed to hypoxia. This suggests that our targeted CRISPR/Cas9 genome editing blocks the hypoxia induced accumulation of HIF-1α, thus its nuclear localization and heterodimerization with HIF-1β is also hindered.

Tissue Engineering
CRISPR/Cas9 edited hiPSC-based vascular tissues to model aging and disease-dependent impairment (DOI: 10.1089/ten.TEA.2018.0271)
This paper has been peer-reviewed and accepted for publication, but has yet to undergo copyediting and proof correction. The final published version may differ from this proof.

CRISPR/Cas9 editing of iECs for HIF-1α knockout interferes with migration and tube formation

HIF-1 expression is known to drive angiogenesis under ischemic conditions and the age-dependent decrease in its expression is linked with deterioration in endothelial function. Therefore, we determined the migration and tube formation of HIF-1α knockout iECs under ischemia. We observed that when we introduce a scratch in a confluent culture of iECs, regardless of oxygen concentration, HIF-1α knockout iECs covered less area compared to controls (Figure 3A-C) at the end of 18 hours. Strikingly, under ischemia, HIF-1α knockout cell lines covered only 20% of the scratch area. Migration of HUVECs and HIF-$1\alpha^{WT}$ iECs was also affected by ischemia treatment as the approximate area covered decreased from 80% to 40%.

We also quantified the number of cells that migrated to the scratch area under both normoxia and hypoxia (Figure 3D). We observed that for all cell lines there was a significant decrease in cell number migrated to scratch area under ischemic conditions, compared to normoxic conditions. When we determined the percent decrease in number of cells in scratch area caused by ischemia, however, we observed a significant difference in the percent decrease in HIF-1α knockout iECs and controls, indicating that decreased expression of HIF-1α interferes with endothelial migration potential under ischemia.

Tube formation is another indicator of angiogenic potential of endothelial cells. We investigated the number of complete tube-like structures formed by HUVECs, HIF-$1\alpha^{WT}$ iECs, and CRISPR/Cas9 edited iECs under normoxia and ischemia (Figure 3E). When cultured under normoxic conditions, the number of tubes formed by HIF-$1\alpha^{\Delta 19}$ and HIF-$1\alpha^{\Delta 42}$ iECs was comparable to that of HUVECs and HIF-$1\alpha^{WT}$ iECs. At the end of 16 h long ischemia treatment HUVECs and HIF-$1\alpha^{WT}$ iECs were induced to form a significantly higher number of tubes (Figure 3E, F). Interestingly, tube number significantly decreased in both HIF-$1\alpha^{\Delta 19}$ and HIF-$1\alpha^{\Delta 42}$ iECs under ischemia, showing significant impairment in tube formation.

HIF-1α absence significantly affects the viability of iECs through increased mitochondrial ROS accumulation

Reduction in mitochondrial ROS has been shown to be regulated by HIF-1 through the induction of pyruvate dehydrogenase kinase-1 (PDK-1) under hypoxia[30–32] leading to decreased cell death. In addition, it is well-documented that there is an age-dependent increase in susceptibility to stresses such as ischemia. Therefore, we characterized the functionality of our CRISPR/Cas9 edited iECs through investigating the accumulation of mitochondrial ROS and cell viability on 2D and 3D (Figure 4A). At the end of 96 h ischemia treatment the HIF-1α knockout iECs cultured as 2D monolayers showed an increase in mitochondrial ROS levels compared to ones cultured in normoxia (Figure 4B). However, the mitochondrial ROS levels did not change in HUVECs and HIF-1α^{WT} iECs whether they were cultured under normoxia or ischemia, suggesting that CRISPR/Cas9 edited iECs cannot maintain the HIF-1α regulated mitochondrial oxygen balance. We investigated the cell viability after 96 h ischemia treatment (Figure 4C) and observed that, all cell lines were over 90% viable under normoxia. However, in correlation with ROS accumulation, HUVECs, HIF-1α^{WT} iECs, and HIF-1α knockout cells showed a significantly lower viability under ischemia (Figure 4D). Importantly, HIF-1$\alpha^{\Delta 19}$ and HIF-1$\alpha^{\Delta 42}$ iECs showed a more significant decrease in viability as a result of ischemia exposure: the viability of HUVECs and HIF-1α^{WT} remained above 75% after ischemia exposure, whereas viability of HIF-1$\alpha^{\Delta 19}$ iECs decreased to 58±7% and viability of HIF-1$\alpha^{\Delta 42}$ iECs decreased to 56±4% under ischemia.

We developed the 3D vascular tissues through encapsulating HIF-1α WT or knockout ECs in GelMA. We first investigated the stress response of our CRISPR/Cas9 edited vascular tissues under ischemia. We exposed the 3D tissues to ischemia for 96 h and observed a significant increase in mitochondrial ROS levels in HIF-1$\alpha^{\Delta 19}$ and HIF-1$\alpha^{\Delta 42}$ vascular tissues while ROS levels did not change with ischemia in HUVECs and HIF-1α^{WT} vascular tissues (Figure 5A, B) in consistence with the 2D cultures. The viability of the tissue models followed a different pattern upon ischemia in 3D compared to 2D culture conditions (Figure 5C, D). The initial viability was over 80% for all tissues and this viability level was maintained in HUVEC and HIF-1α^{WT} vascular tissue models following ischemia treatment

(Figure 5D). However, viability of HIF-1$\alpha^{\Delta 19}$ and HIF-1$\alpha^{\Delta 42}$ vascular tissues decreased significantly.

HIF-1α knockout iECs are unable to form lumens mimicking angiogenic deterioration

We determined the 3D angiogenic potential of our CRISPR/Cas9 edited vascular tissues under normoxia and ischemia. We observed that both HUVECs and iECs could spread and form lumens under normoxia (Supplementary Figure 1) and hypoxia (Figure 6A) through 14 days of culture.

By day 14 completely connected lumen-like structures were formed regardless of HIF-1α expression (Supplementary Figure 2). The quantification of lumen number (Figure 6B, C) showed that a lower number of lumens were formed in HIF-1$\alpha^{\Delta 19}$ and HIF-1$\alpha^{\Delta 42}$ vascular tissues compared to HUVEC and HIF-1α^{WT} iEC tissues, but this difference was statistically insignificant (Figure 6B). Under ischemia, the number of lumens formed in HUVEC and HIF-1α^{WT} vascular tissues significantly increased, compared to normoxia, whereas HIF-1$\alpha^{\Delta 19}$ and HIF-1$\alpha^{\Delta 42}$ vascular tissues had a lower number of lumens under ischemia, compared to normoxia. We also observed that the lumen diameter was smaller in all tissue models under ischemia, compared to normoxia (Figure 6C). Taken together, our results show that a higher number of lumens with smaller diameter are formed in the HUVEC and HIF-1α^{WT} vascular tissue models under ischemia. Similarly, the lumen diameter significantly decreased in tissues comprised of edited iEC under ischemia, however, the number of lumens formed remained the same.

Discussion

Construction of in vitro disease models using primary human cells is disadvantageous as these cells are not readily available, especially for vital organs such as heart and brain. The animal models provide a platform where the systemic effect of potential therapeutics can be assessed, however, the species to species differences and physiologically inaccurate methods often used to create the disease conditions hinder their translational value. The discovery of hiPSCs and the advancements in the past decade brought upon new possibilities for disease modeling while overcoming many of the disadvantages the preexisting methods have. With the use of hiPSCs many different cell types have been

Tissue Engineering
CRISPR/Cas9 edited hiPSC-based vascular tissues to model aging and disease-dependent impairment (DOI: 10.1089/ten.TEA.2018.0271)
This paper has been peer-reviewed and accepted for publication, but has yet to undergo copyediting and proof correction. The final published version may differ from this proof.

Tissue Engineering
CRISPR/Cas9 edited hiPSC-based vascular tissues to model aging and disease-dependent impairment (DOI: 10.1089/ten.TEA.2018.0271)
This paper has been peer-reviewed and accepted for publication, but has yet to undergo copyediting and proof correction. The final published version may differ from this proof.

successfully derived to date[33]. Combined with the advancements in genome editing technology, it is now possible to model human diseases in a physiologically, pathologically, and genetically relevant manner [6,8,34,35].

Deterioration in angiogenesis is associated with many diseases such as arteriosclerosis, myocardial infarction, and limb ischemia[36]. The age-dependent impairment in angiogenesis and neovascularization, as well as an increased susceptibility to stress have been reported to be directly correlated with a decrease in stabilization[25] or nuclear localization of HIF-1α[24]. Despite its great importance in age-related ischemic diseases, in vitro tissue models that mimic the impaired vascular tissues both on genetic and functional level were not reported. In this study, we developed hiPSC-based vascular tissues that show the functional impairment observed in an age-relevant manner through CRISPR/Cas9 editing of HIF-1α.

We employed CRISPR/Cas9 editing to knockout HIF-1α in ECs as it is shown to yield the highest efficiency in genome editing[3,37,385]. CRISPR/Cas9 genome editing yielded both homozygous and heterozygous deletions in the second exon of *HIF-1A.* The cell lines with homozygous deletions showed significantly decreased mRNA and protein levels of HIF-1α in hiPSCs. The respective iECs derived from the edited cell lines showed characteristic endothelial biochemical marker expression and functionality, while maintaining the significant decrease in HIF-1α mRNA and protein levels, indicating no interference of genome editing with the differentiation potential of hiPSCs. HUVECs and HIF-1α^{WT} iECs showed the expected increase in HIF-1α protein expression under ischemia, while the genome edited iECs maintained the protein expression level that was observed under normoxia. This suggests that although mRNA and protein expression are not completely hindered due to the deletions introduced via CRISPR/Cas9 editing, the oxygen-dependent stabilization of HIF-1α expression is blocked, presenting edited iECs as a viable model of HIF-1α knockout. This could be due to the shift introduced by the deletion overall affecting the oxygen-dependent degradation domain of HIF-1α which is located downstream of bHLH and PAS domains and mediates its oxygen-regulated stability[39].

Tissue Engineering
CRISPR/Cas9 edited hiPSC-based vascular tissues to model aging and disease-dependent impairment (DOI: 10.1089/ten.TEA.2018.0271)
This paper has been peer-reviewed and accepted for publication, but has yet to undergo copyediting and proof correction. The final published version may differ from this proof.

We observed that CRISPR/Cas9 editing of iECs to knockout HIF-1α resulted in a decrease in migration and tube formation, resembling the age-dependent impairment in angiogenesis[24] and recruitment of ECs under ischemia[25]. In line with other reports[40,41] angiogenic response of HUVECs and HIF-1α^{WT} iECs was induced under ischemia as shown by increased number of tubes formed, while HIF-1α knockout iECs formed lower number of tubes compared to normoxia. This strongly suggests that in the absence of HIF-1α expression, iECs have impaired functionality.

An important player in ischemia-related cell death is the mitochondrial ROS generation and accumulation[42]. In correlation with decreased tube formation, we observed an increased accumulation of mitochondrial ROS in HIF-1α$^{\Delta 19}$ and HIF-1α$^{\Delta 42}$ iECs under ischemia in 2D cultures. HIF-1 expression is documented to improve survival under hypoxic conditions through induction of PDK-1, which blocks the entry of pyruvate into the tricarboxylic acid (TCA) cycle and subsequently suppresses mitochondrial ROS production[32]. Therefore, CRISPR/Cas9 knockout of HIF-1α in iECs lead to the accumulation of mitochondrial ROS and subsequently to a lower survival rate when cultured in 2D. Importantly, observing a decrease in tube formation in knockout iECs can be attributed to the accumulation of mitochondrial ROS and the correlated lower overall viability. In addition, the deletion we introduced targets the bHLH domain of HIF-1α, which regulates the dimerization with HIF-1β, thus the activity of HIF-1 as a transcription factor[39]. It is well documented that VEGF expression is regulated by HIF-1 under hypoxia to induce angiogenesis and tube formation of ECs[43–45]. Therefore, in addition to mitochondrial ROS accumulation, the transcriptional pathways activated by HIF-1 are impaired in CRISPR/Cas9 edited iECs which collectively could lead to the observed decrease in migration, tube formation, and viability.

Although the conventional 2D cultures provide valuable information, cell-microenvironment interactions are overlooked in such platforms. To remedy this, 3D tissue and disease models have been developed over the years[46]. Cell-laden hydrogel-based tissue model fabrication is a common approach to create 3D tissue models and collagen and gelatin-based hydrogels have been documented to support various cell types[47–50], including endothelial cell culture and function in vitro[47,51–54]. We encapsulated the HIF-1α

Tissue Engineering
CRISPR/Cas9 edited hiPSC-based vascular tissues to model aging and disease-dependent impairment (DOI: 10.1089/ten.TEA.2018.0271)
This paper has been peer-reviewed and accepted for publication, but has yet to undergo copyediting and proof correction. The final published version may differ from this proof.

knockout and WT ECs in photocrosslinkable GelMA to provide cell-ECM interactions as well as improving cell-cell interactions provided with the 3D architecture. The 3D tissue models comprising HUVECs and HIF-1α^{WT} iECs could survive the ischemia treatment, unlike observed in the 2D culture conditions. This can be explained by the well-documented effect of improved cell-ECM and cell-cell interactions provided in our 3D constructs[14,55]. However, when HIF-1α was knocked out in iECs, improved cell-cell and cell-ECM interactions provided by the 3D architecture was not enough to improve the survival of the tissue models under ischemia treatment. This is in line with our previous studies where HIF-1α knockdown iECs did not show the same cardioprotective effect as HIF-1α^{WT} iECs under oxidative stress[14]. In addition, the mitochondrial ROS accumulation we observed under ischemia showed a similar pattern to viability of the tissues. HUVEC and HIF-1α^{WT} iEC-laden tissues maintained their mitochondrial ROS levels under ischemia while HIF-1α knockout iEC tissues showed increased ROS accumulation. Thus, the lower viability of edited iECs under ischemia can be explained by the significant increase in ROS accumulation, linking the lack of HIF-1α directly to cell viability under ischemic stress.

Similar to the decreased tube formation on 2D, CRISPR/Cas9 edited iECs showed an impairment in 3D lumen formation resembling the age-dependent deterioration of angiogenic potential of several organs in vivo[36,56]. Overall, the increased mitochondrial ROS accumulation, decreased lumen formation, viability, tube formation, and cell migration show that the CRISPR/Cas9 edited iECs we present in this study are biochemically and functionally resemble the impaired endothelium phenotype that is observed in aged tissues and organs as well as disease conditions.

Using CRISPR/Cas9 edited hiPSCs to develop both 2D and 3D vascular tissues, we have shown here the applicability of the combination of these two techniques in fabricating fully human-origin, physiologically and pathologically-relevant tissue and disease models. The model presented here can be further improved by integrating the parenchymal cells of the target tissue, and diseased and/or aged tissue models can be fabricated for various bioengineering and biomedical applications. Such tissues hold promise to provide more relevant information on tissue/organ pathology and eventually will lead to developing successful treatments.

Acknowledgements

This study is funded by NSF-CAREER Award No. 1651385, NSFCBET Award No. 1805157, NIH Award No 1 R01 HL141909-01A1.

Disclosure

No competing financial interests exist.

Tissue Engineering
CRISPR/Cas9 edited hiPSC-based vascular tissues to model aging and disease-dependent impairment (DOI: 10.1089/ten.TEA.2018.0271)
This paper has been peer-reviewed and accepted for publication, but has yet to undergo copyediting and proof correction. The final published version may differ from this proof.

References

1. Wang, H.-X. *et al.* CRISPR/Cas9-Based Genome Editing for Disease Modeling and Therapy: Challenges and Opportunities for Nonviral Delivery. *Chem. Rev.* **117**, 9874–9906 (2017).

2. Gaj, T., Gersbach, C. A. & Barbas, C. F. ZFN, TALEN, and CRISPR/Cas-based methods for genome engineering. *Trends Biotechnol.* **31**, 397–405 (2013).

3. Dow, L. E. Modeling Disease In Vivo With CRISPR/Cas9. *Trends Mol. Med.* **21**, 609–621 (2015).

4. Wu, Y. *et al.* Correction of a Genetic Disease in Mouse via Use of CRISPR-Cas9. *Cell Stem Cell* **13**, 659–662 (2013).

5. Yin, H. *et al.* Genome editing with Cas9 in adult mice corrects a disease mutation and phenotype. *Nat. Biotechnol.* **32**, 551–553 (2014).

6. Freedman, B. S. *et al.* Modelling kidney disease with CRISPR-mutant kidney organoids derived from human pluripotent epiblast spheroids. *Nat. Commun.* **6**, 8715 (2015).

7. Flynn, R. *et al.* CRISPR-mediated genotypic and phenotypic correction of a chronic granulomatous disease mutation in human iPS cells. *Exp. Hematol.* **43**, 838-848.e3 (2015).

8. Wang, G. *et al.* Modeling the mitochondrial cardiomyopathy of Barth syndrome with induced pluripotent stem cell and heart-on-chip technologies. *Nat. Med.* **20**, 616–623 (2014).

9. Yang, S. *et al.* CRISPR/Cas9-mediated gene editing ameliorates neurotoxicity in mouse model of Huntington's disease. *J. Clin. Invest.* **127**, 2719–2724 (2017).

10. Ong, S.-G. & Hausenloy, D. J. Hypoxia-inducible factor as a therapeutic target for cardioprotection. *Pharmacol. Ther.* **136**, 69–81 (2012).

11. Heyman, S. N., Rosen, S. & Rosenberger, C. Hypoxia-inducible factors and the prevention of acute organ injury. *Crit. Care Lond. Engl.* **15**, 209 (2011).

12. Shohet, R. V. & Garcia, J. A. Keeping the engine primed: HIF factors as key regulators of cardiac metabolism and angiogenesis during ischemia. *J. Mol. Med. Berl. Ger.* **85**, 1309–1315 (2007).

13. Pugh, C. W. & Ratcliffe, P. J. Regulation of angiogenesis by hypoxia: role of the HIF system. *Nat. Med.* **9**, 677–684 (2003).

14. Acun, A. & Zorlutuna, P. Engineered myocardium model to study the roles of HIF-1α and HIF1A-AS1 in paracrine-only signaling under pathological level oxidative stress. *Acta Biomater.* **58**, 323–336 (2017).

15. Yue, X., Acun, A. & Zorlutuna, P. Transcriptome profiling of 3D co-cultured cardiomyocytes and endothelial cells under oxidative stress using a photocrosslinkable hydrogel system. *Acta Biomater.* **58**, 337–348 (2017).

16. Eckle, T., Köhler, D., Lehmann, R., El Kasmi, K. & Eltzschig, H. K. Hypoxia-inducible factor-1 is central to cardioprotection: a new paradigm for ischemic preconditioning. *Circulation* **118**, 166–175 (2008).

17. Li, D. F. *et al.* Induction of microRNA-24 by HIF-1 protects against ischemic injury in rat cardiomyocytes. *Physiol. Res.* **61**, 555–565 (2012).

18. Bernaudin, M. *et al.* Normobaric Hypoxia Induces Tolerance to Focal Permanent Cerebral Ischemia in Association with an Increased Expression of Hypoxia-Inducible Factor-1 and its Target Genes, Erythropoietin and VEGF, in the Adult Mouse Brain. *J. Cereb. Blood Flow Metab.* **22**, 393–403 (2002).

19. Marti, H. J. H. *et al.* Hypoxia-Induced Vascular Endothelial Growth Factor Expression Precedes Neovascularization after Cerebral Ischemia. *Am. J. Pathol.* **156**, 965–976 (2000).

20. Semenza, G. L. HIF-1 and human disease: one highly involved factor. *Genes Dev.* **14**, 1983–1991 (2000).

21. Ma, D. *et al.* Xenon Preconditioning Protects against Renal Ischemic-Reperfusion Injury via HIF-1α Activation. *J. Am. Soc. Nephrol.* **20**, 713–720 (2009).

22. Conde, E. *et al.* Hypoxia Inducible Factor 1-Alpha (HIF-1 Alpha) Is Induced during Reperfusion after Renal Ischemia and Is Critical for Proximal Tubule Cell Survival. *PLOS ONE* **7**, e33258 (2012).

23. Ho, T. K. *et al.* Increased endogenous angiogenic response and hypoxia-inducible factor-1alpha in human critical limb ischemia. *J. Vasc. Surg.* **43**, 125–133 (2006).

Tissue Engineering
CRISPR/Cas9 edited hiPSC-based vascular tissues to model aging and disease-dependent impairment (DOI: 10.1089/ten.TEA.2018.0271)
This paper has been peer-reviewed and accepted for publication, but has yet to undergo copyediting and proof correction. The final published version may differ from this proof.

24. Ahluwalia, A., Narula, J., Jones, M. K., Deng, X. & Tarnawski, A. S. Impaired angiogenesis in aging myocardial microvascular endothelial cells is associated with reduced importin alpha and decreased nuclear transport of HIF1 alpha: mechanistic implications. *J. Physiol. Pharmacol. Off. J. Pol. Physiol. Soc.* **61**, 133–139 (2010).

25. Chang, E. I. *et al.* Age decreases endothelial progenitor cell recruitment through decreases in hypoxia-inducible factor 1alpha stabilization during ischemia. *Circulation* **116**, 2818–2829 (2007).

26. Peters, D. T., Cowan, C. A. & Musunuru, K. Genome editing in human pluripotent stem cells. in *StemBook* (Harvard Stem Cell Institute, 2008).

27. Patsch, C. *et al.* Generation of vascular endothelial and smooth muscle cells from human pluripotent stem cells. *Nat. Cell Biol.* **17**, 994–1003 (2015).

28. Ellis, B. W., Acun, A., Can, U. I. & Zorlutuna, P. Human iPSC-derived myocardium-on-chip with capillary-like flow for personalized medicine. *Biomicrofluidics* **11**, 024105 (2017).

29. Iyer, N. V., Leung, S. W. & Semenza, G. L. The human hypoxia-inducible factor 1alpha gene: HIF1A structure and evolutionary conservation. *Genomics* **52**, 159–165 (1998).

30. Kim, J., Tchernyshyov, I., Semenza, G. L. & Dang, C. V. HIF-1-mediated expression of pyruvate dehydrogenase kinase: A metabolic switch required for cellular adaptation to hypoxia. *Cell Metab.* **3**, 177–185 (2006).

31. Papandreou, I., Cairns, R. A., Fontana, L., Lim, A. L. & Denko, N. C. HIF-1 mediates adaptation to hypoxia by actively downregulating mitochondrial oxygen consumption. *Cell Metab.* **3**, 187–197 (2006).

32. Kirito, K., Hu, Y. & Komatsu, N. HIF-1 prevents the overproduction of mitochondrial ROS after cytokine stimulation through induction of PDK-1. *Cell Cycle* **8**, 2844–2849 (2009).

33. Singh, V. K., Kalsan, M., Kumar, N., Saini, A. & Chandra, R. Induced pluripotent stem cells: applications in regenerative medicine, disease modeling, and drug discovery. *Front. Cell Dev. Biol.* **3**, (2015).

34. Hockemeyer, D. & Jaenisch, R. Induced pluripotent stem cells meet genome editing. *Cell Stem Cell* **18**, 573–586 (2016).

35. Carvajal-Vergara, X. *et al.* Patient-specific induced pluripotent stem-cell-derived models of LEOPARD syndrome. *Nature* **465**, 808–812 (2010).

36. Storgard, C. M. *et al.* Decreased angiogenesis and arthritic disease in rabbits treated with an αvβ3 antagonist. *J. Clin. Invest.* **103**, 47–54 (1999).

37. Smith, C. *et al.* Whole-Genome Sequencing Analysis Reveals High Specificity of CRISPR/Cas9 and TALEN-Based Genome Editing in Human iPSCs. *Cell Stem Cell* **15**, 12–13 (2014).

38. Cong, L. *et al.* Multiplex genome engineering using CRISPR/Cas systems. *Science* **339**, 819–823 (2013).

39. Ke, Q. & Costa, M. Hypoxia-Inducible Factor-1 (HIF-1). *Mol. Pharmacol.* **70**, 1469–1480 (2006).

40. Kroon, M. E., Koolwijk, P., Vecht, B. van der & Hinsbergh, V. W. M. van. Urokinase receptor expression on human microvascular endothelial cells is increased by hypoxia: implications for capillary-like tube formation in a fibrin matrix. *Blood* **96**, 2775–2783 (2000).

41. Manalo, D. J. *et al.* Transcriptional regulation of vascular endothelial cell responses to hypoxia by HIF-1. *Blood* **105**, 659–669 (2005).

42. Levraut, J., Iwase, H., Shao, Z.-H., Vanden Hoek, T. L. & Schumacker, P. T. Cell death during ischemia: relationship to mitochondrial depolarization and ROS generation. *Am. J. Physiol.-Heart Circ. Physiol.* **284**, H549–H558 (2003).

43. Forsythe, J. A. *et al.* Activation of vascular endothelial growth factor gene transcription by hypoxia-inducible factor 1. *Mol. Cell. Biol.* **16**, 4604–4613 (1996).

44. Yamakawa, M. *et al.* Hypoxia-Inducible Factor-1 Mediates Activation of Cultured Vascular Endothelial Cells by Inducing Multiple Angiogenic Factors. *Circ. Res.* (2003).

45. Tang, N. *et al.* Loss of HIF-1α in endothelial cells disrupts a hypoxia-driven VEGF autocrine loop necessary for tumorigenesis. *Cancer Cell* **6**, 485–495 (2004).

46. Huh, D., Hamilton, G. A. & Ingber, D. E. From 3D cell culture to organs-on-chips. *Trends Cell Biol.* **21**, 745–754 (2011).

47. Prakash Parthiban, S., Rana, D., Jabbari, E., Benkirane-Jessel, N. & Ramalingam, M. Covalently immobilized VEGF-mimicking peptide with gelatin methacrylate enhances microvascularization of endothelial cells. *Acta Biomater.* **51**, 330–340 (2017).

48. Arya, A. D. *et al.* Gelatin Methacrylate Hydrogels as Biomimetic Three-Dimensional Matrixes for Modeling Breast Cancer Invasion and Chemoresponse in Vitro. *ACS Appl. Mater. Interfaces* **8**, 22005–22017 (2016).

49. Nichol, J. W. *et al.* Cell-laden microengineered gelatin methacrylate hydrogels. *Biomaterials* **31**, 5536–5544 (2010).

50. Ramón-Azcón, J. *et al.* Gelatin methacrylate as a promising hydrogel for 3D microscale organization and proliferation of dielectrophoretically patterned cells. *Lab. Chip* **12**, 2959–2959 (2012).

51. Chan, T. R., Stahl, P. J., Li, Y. & Yu, S. M. Collagen–gelatin mixtures as wound model, and substrates for VEGF-mimetic peptide binding and endothelial cell activation. *Acta Biomater.* **15**, 164–172 (2015).

52. Wenz, A., Tjoeng, I., Schneider, I., Kluger, P. J. & Borchers, K. Improved vasculogenesis and bone matrix formation through coculture of endothelial cells and stem cells in tissue-specific methacryloyl gelatin-based hydrogels. *Biotechnol. Bioeng.* **0**,

53. Ramamoorthy, S., Bertucci, C. P., Thompson, D. M. & Karande, P. High throughput screening of endothelial cell response to combinatorial collagen - matrigel biomaterials. in *2015 41st Annual Northeast Biomedical Engineering Conference (NEBEC)* 1–2 (2015). doi:10.1109/NEBEC.2015.7117123

54. Goto, F., Goto, K., Weindel, K. & Folkman, J. Synergistic effects of vascular endothelial growth factor and basic fibroblast growth factor on the proliferation and cord formation of bovine capillary endothelial cells within collagen gels. *Lab. Investig. J. Tech. Methods Pathol.* **69**, 508–517 (1993).

55. Sun, T., Jackson, S., Haycock, J. W. & MacNeil, S. Culture of skin cells in 3D rather than 2D improves their ability to survive exposure to cytotoxic agents. *J. Biotechnol.* **122**, 372–381 (2006).

56. Kang, D.-H. *et al.* Impaired angiogenesis in the aging kidney: Vascular endothelial growth factor and Thrombospondin-1 in renal disease. *Am. J. Kidney Dis.* **37**, 601–611 (2001).

Tissue Engineering
CRISPR/Cas9 edited hiPSC-based vascular tissues to model aging and disease-dependent impairment (DOI: 10.1089/ten.TEA.2018.0271)
This paper has been peer-reviewed and accepted for publication, but has yet to undergo copyediting and proof correction. The final published version may differ from this proof.

Reprint Author:

Pinar Zorlutuna

143 Multidisciplinary Research Building Notre Dame, IN, 46556

Email: Pinar.Zorlutuna.1@nd.edu

Phone: 574-631-8543

Tissue Engineering
CRISPR/Cas9 edited hiPSC-based vascular tissues to model aging and disease-dependent impairment (DOI: 10.1089/ten.TEA.2018.0271)
This paper has been peer-reviewed and accepted for publication, but has yet to undergo copyediting and proof correction. The final published version may differ from this proof.

Figure Legends

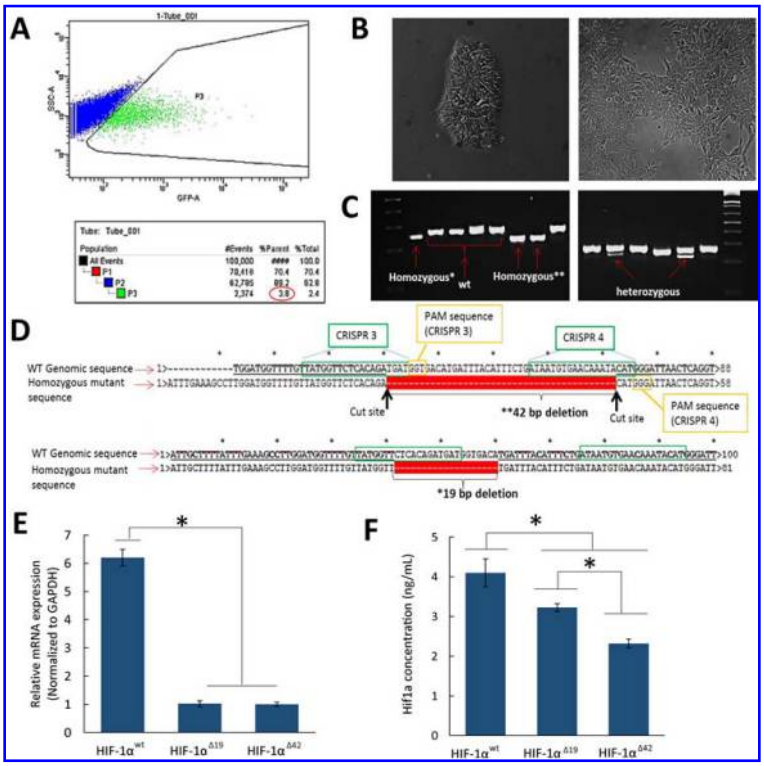

Figure 1. Characterization of CRISPR/Cas9 edited iPSCs (A) FACS results of Cas9 plasmid transfection efficiency in hiPSCs. (B) The bright field images of iPSC colonies (left) and their expansion for genome screening (right). (C) The PCR results showing the homozygous and heterozygous colonies with genetic modification in *HIF-1A.* (D) The sequencing results showing the deletions in *HIF-1A* and the respective CRISPR cut sites. (E) The HIF-1α mRNA levels in WT and edited hiPSCs under hypoxia. (F) The HIF-1a protein concentration in WT and edited hiPSCs under hypoxia. (* represents statistical significance ($p<0.05$)).

Tissue Engineering
CRISPR/Cas9 edited hiPSC-based vascular tissues to model aging and disease-dependent impairment (DOI: 10.1089/ten.TEA.2018.0271)
This paper has been peer-reviewed and accepted for publication, but has yet to undergo copyediting and proof correction. The final published version may differ from this proof.

Tissue Engineering
CRISPR/Cas9 edited hiPSC-based vascular tissues to model aging and disease-dependent impairment (DOI: 10.1089/ten.TEA.2018.0271)

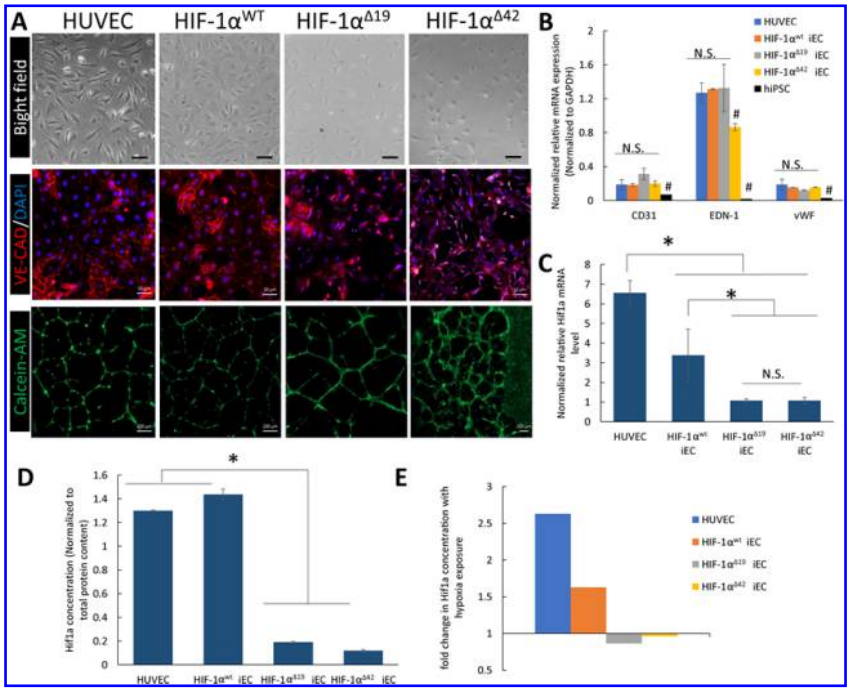

Figure 2. Biochemical characterization of HIF-1α knockout iECs. (A) Top: The bright field images of HUVECs and iECs (day after FACS sorting) (Scale bars=50 μm). Middle: Immunostaining of HUVECs and iECs against VE-CAD (the cell nuceli are labeled with DAPI) (Scale bars=50 μm). Bottom: The tube formation by HUVECs and iECs under normoxia (cells are labeled with calcein-AM) (Scale bars=200 μm). (B) The mRNA expression levels of endothelial markers CD31, EDN-1, and vWF in HUVECs, iECs and undifferentiated iPSCs under normoxia. (C) The HIF-1α mRNA levels in HUVECs and iECs under hypoxia (the expression levels are normalized to the respective expression levels of the same cell line under normoxia) as determined by qRT-PCR. (D) The HIF-1α protein concentration in HUVECs and iECs under hypoxia. (E) The fold difference in HIF-1α protein concentration (hypoxia protein levels)/(normoxia protein level). (* represents statistical significance ($p<0.05$); # represents statistical significance when mRNA expression of a gene is compared to other cell lines ($p<0.05$); N.S. represents no statistical significance ($p>0.05$))

Tissue Engineering
CRISPR/Cas9 edited hiPSC-based vascular tissues to model aging and disease-dependent impairment (DOI: 10.1089/ten.TEA.2018.0271)
This paper has been peer-reviewed and accepted for publication, but has yet to undergo copyediting and proof correction. The final published version may differ from this proof.

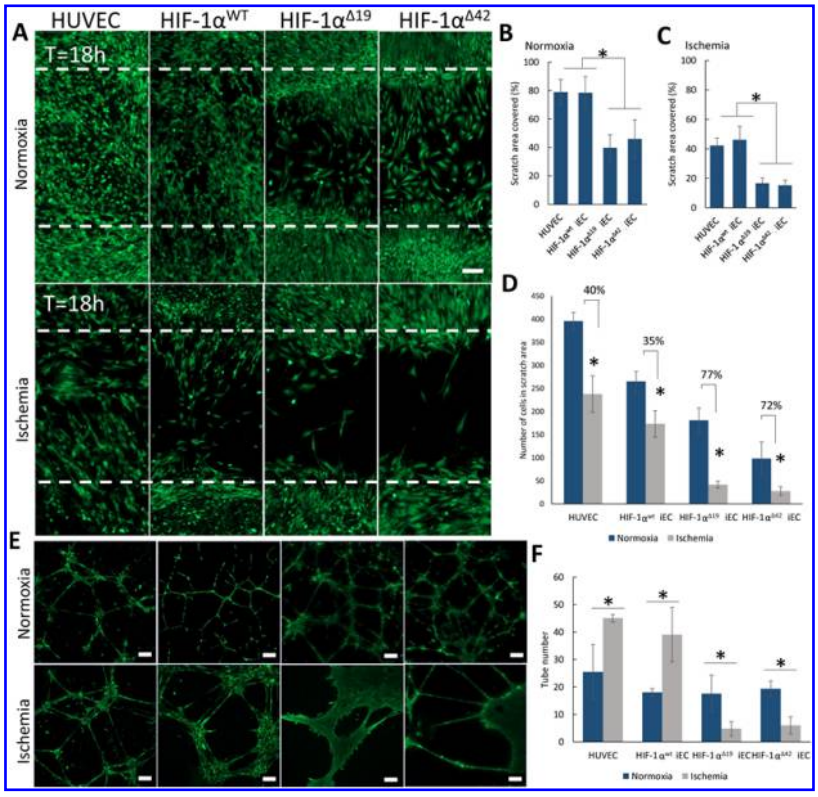

Figure 3. Migration and angiogenic potential of CRISPR/Cas9 edited iECs. (A) Fluorescent images showing the migration of HUVECs and iECs to the scratch area at the end of 18 hours under normoxia (top) and ischemia (bottom). Cells are labeled with calcein-AM. (Scale bar=200 µm) (B) The percentage of scratch area covered at the end of 18 h under normoxia and (C) ischemia. (D) The cell number in the scratch area under normoxia and ischemia. The percent difference in cell number under normoxia and ischemia for each cell line is represented on top of the respective bars. (E) The fluorescent images of HUVECs and iECs forming tube-like structures under normoxia and ischemia. (Scale bar=100 µm) (F) The quantification of the tubing assay showing the number of complete tubes formed by HUVECs and iECs under normoxia and ischemia. (* represents statistical significance ($p<0.05$))

Tissue Engineering
CRISPR/Cas9 edited hiPSC-based vascular tissues to model aging and disease-dependent impairment (DOI: 10.1089/ten.TEA.2018.0271)
This paper has been peer-reviewed and accepted for publication, but has yet to undergo copyediting and proof correction. The final published version may differ from this proof.

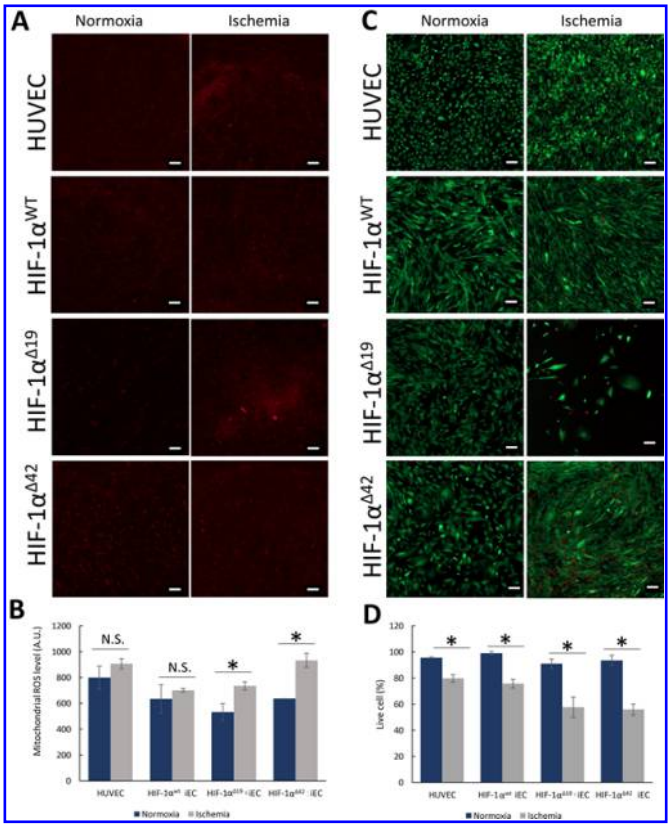

Figure 4. Mitochondrial ROS accumulation and cell viability in CRISPR/Cas9 edited iECs in 2D. (A) the representative images and (B) quantification of mitochondrial ROS in HUVECs and iECs under normoxia and ischemia. (mitochondrial ROS is represented by fluorescence intensity, in arbitrary units (A.U.)). (Scale bars=100 µm) (C) The representative images and (D) quantification of live/dead assay (represented as live cell percentage) of HUVECs and iECs under normoxia and ischemia. (Scale bars=100 µm) (* represents statistical significance ($p<0.05$); N.S. represents no statistical significance ($p>0.05$))

Tissue Engineering
CRISPR/Cas9 edited hiPSC-based vascular tissues to model aging and disease-dependent impairment (DOI: 10.1089/ten.TEA.2018.0271)
This paper has been peer-reviewed and accepted for publication, but has yet to undergo copyediting and proof correction. The final published version may differ from this proof.

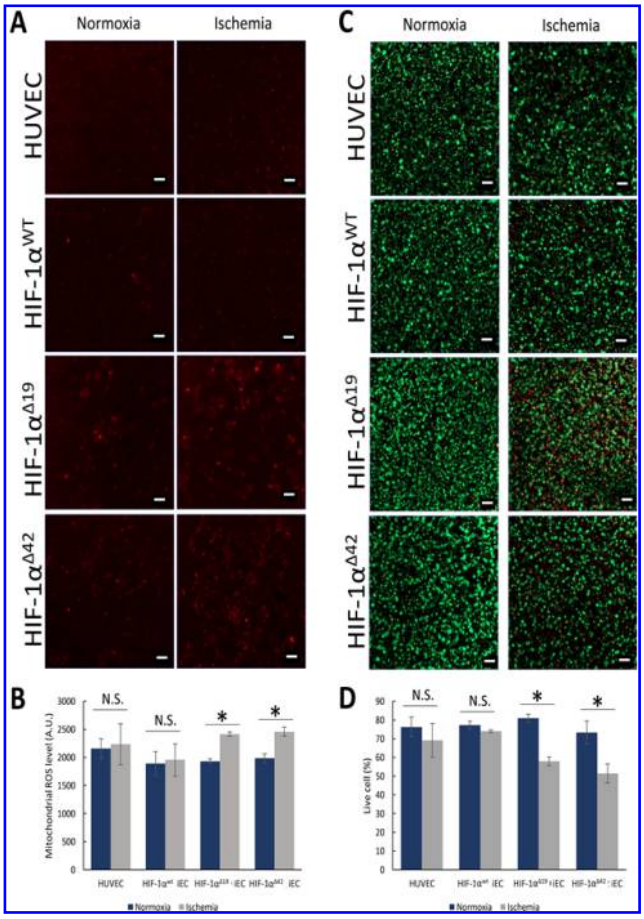

Figure 5. Mitochondrial ROS accumulation and cell viability in CRISPR/Cas9 edited iECs in 3D. (A) The representative images and (B) quantification of mitochondrial ROS in HUVECs and iECs encapsulated in GelMA under normoxia and ischemia. (mitochondrial ROS is represented by fluorescence intensity, in arbitrary units (A.U.)). (Scale bars=100 µm) (C) The representative images and (D) quantification of live/dead assay (represented as live cell percentage) HUVECs and iECs encapsulated in GelMA under normoxia and ischemia. (Scale bars=100 µm) (* represents statistical significance ($p<0.05$); N.S. represents no statistical significance ($p>0.05$))

Tissue Engineering
CRISPR/Cas9 edited hiPSC-based vascular tissues to model aging and disease-dependent impairment (DOI: 10.1089/ten.TEA.2018.0271)

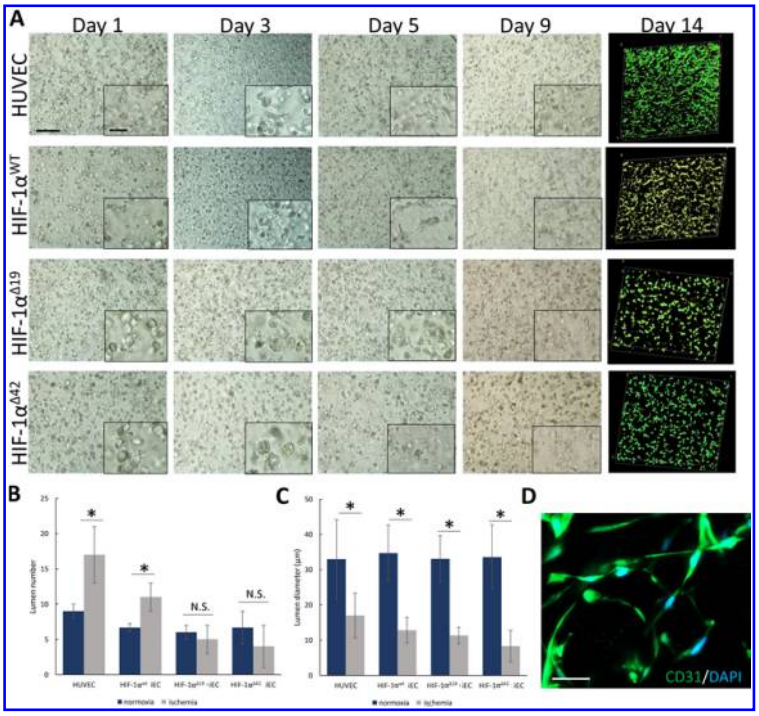

Figure 6. Lumen formation of CRISPR/Cas9 edited iECs under normoxia and ischemia. (A) Bright field (days 1, 3, 5, 9) and fluorescent images (day 14) of 3D lumen formation of HUVECs and iECs under ischemia. (Scale bar=100 µm, inset scale bar=50 µm) (B) The number of complete lumens formed per construct under normoxia and ischemia. (C) The diameter of lumens formed under normoxia and ischemia. (D) A close-up image of 3D lumen formation of HUVECs under ischemia. (Scale bar=100 µm) (* represents statistical significance ($p<0.05$); N.S. represents no statistical significance ($p>0.05$))